Available online at www.sciencedirect.com
SCIENCE DIRECT®
Journal of Solid State Chemistry 175 (2003) 207–217
JOURNAL OF SOLID STATE CHEMISTRY
http://elsevier.com/locate/jssc

Structural properties of $La_xSr_{2-x}FeO_{4\pm\delta}$ at high temperature and under reducing conditions

A.J. Jennings,[a] S.J. Skinner,[a,*] and Ö. Helgason[b]

[a] *Department of Materials, Royal School of Mines, Imperial College London,, Prince Consort Road, London SW7 2BP, UK*
[b] *Science Institute, University of Iceland, Dunhagi 3, Reykjavik IS-107, Iceland*

Received 18 November 2002; received in revised form 24 February 2003; accepted 29 April 2003

Abstract

A series of materials, $La_xSr_{2-x}FeO_{4\pm\delta}$ ($x = 0.6-1.0$), have been investigated structurally using neutron and X-ray diffraction techniques as well as Mössbauer spectroscopy as a function of temperature and composition. These materials adopt the $I4/mmm$ K_2NiF_4-type structure over a wide range of temperatures (25–1200°C) and oxygen stoichiometries. In particular, it was observed that at a critical composition of $x > 0.8$ there was a significant shift in the lattice parameters. This was attributed to changes in the Fe^{3+} content and the resultant effect of this on the d_z^2 orbitals giving a lengthening of the Fe–O bonds. On heating, completely linear behavior in both the a and c cell constants was observed, masking underlying bond length changes.

Keywords: K_2NiF_4; Diffraction; In situ; Structure; Stability

1. Introduction

Development of fuel cell technology is rapidly expanding and with basic materials identified and early commercial devices in production the challenge now is to find potential new materials which function more efficiently, are cheaper to produce or offer enhanced thermomechanical efficiency. A recent development in fuel cell cathode technology has been the development of interstitial oxide ion conducting materials and several authors have investigated the K_2NiF_4-type oxides $La_2NiO_{4+\delta}$ and $La_{2-x}Sr_xNiO_{4+\delta}$ which have been identified as readily incorporating interstitial oxide ions [1–3]. It has been demonstrated that the oxide ions in these materials are highly mobile [1–8] and these authors have discussed the structures adopted, oxygen non-stoichiometry and oxygen ion transport of the doped $La_2NiO_{4+\delta}$ oxides. In particular, Skinner and Kilner [3] determined the oxygen tracer diffusion and surface exchange coefficients of $La_2NiO_{4+\delta}$ and found oxygen diffusion coefficients considerably higher than those reported for $La_{0.6}Sr_{0.4}Co_{0.2}Fe_{0.8}O_3$ (LSCF) at intermediate temperatures (500–700°C) and only one order of magnitude lower than the best perovskite mixed electronic ionic oxide ion conductor, $La_{0.3}Sr_{0.7}CoO_3$ (LSC). The fast oxide ion diffusion of $La_2NiO_{4+\delta}$ and also Co-doped variants [7,8] combined with its thermal stability indicated that materials of this structure type would be good candidates for use in ceramic oxygen generators (COGs) and solid oxide fuel cells (SOFCs).

The aim of the current investigation was to study a related material, $La_xSr_{2-x}FeO_{4\pm\delta}$, which adopts the K_2NiF_4-type structure and is thought to incorporate interstitial oxide ions for the $x = 1$ composition [9,10]. Previous work on these materials prepared by conventional solid-state synthesis from stoichiometric quantities of the oxides and carbonates covered a range of properties at both ambient temperatures and temperatures down to 5 K [11–13]. Little work has been performed at temperatures relevant to solid-state electrochemical devices.

Soubeyroux et al. [12] investigated the structure of $SrLaFeO_4$ at low temperature and, in particular, solved its magnetic structure through neutron diffraction measurements identifying a magnetic unit cell of $a_{mag} = 2a_{cryst}$ and $c_{mag} = c_{cryst}$. Mössbauer spectroscopy of $SrLaFeO_4$ was also performed and identified one single sextet component at 293 K which complemented the work of Shimada et al. [11] who also reported at least

*Corresponding author. Fax: +44-020-7584-3194.
E-mail address: s.skinner@imperial.ac.uk (S.J. Skinner).

0022-4596/03/$ - see front matter © 2003 Elsevier Inc. All rights reserved.
doi:10.1016/S0022-4596(03)00248-2

one magnetic component at 280 K and reported the determination of the Néel temperature to be 330 K. Further results were reported for the Nd, Sm and Pr analogues with similar magnetic properties found. A wider compositional range with $x = 1-2$ was examined by Takeda et al. [13] who investigated the structures and conductivities of these materials reporting the elongation of the Fe–O_6 octahedron with increasing La content and a decrease in the oxygen content at temperatures around 400°C. Omata et al. reported the synthesis of both oxygen excess $LaSrFeO_{4+\delta}$ [9] and $La_{1-x}Sr_{1+x}FeO_4$ and reported on their electrical and magnetic properties [9,10] finding that all compositions were p-type semiconductors [10]. These authors also applied X-ray absorption techniques to the $La_{1-x}Sr_{1+x}FeO_4$ material to further analyze the electronic structure finding that the electrical and magnetic property changes corresponded to the electronic structure changes. These reports deal exclusively with the electronic and magnetic behavior at low temperatures. There have been no studies of these materials at elevated temperatures, particularly on varying the La:Sr ratio. Furthermore there have been no studies of the thermal stability of these materials, both with respect to structural changes and non-stoichiometry, at elevated temperatures.

This work investigates the thermal stability of the $La_xSr_{2-x}FeO_{4\pm\delta}$ materials using in situ X-ray and neutron diffraction at elevated temperatures in air as it is envisaged that any application of these materials in fuel cells would be as a cathode operating in an air environment. Oxygen non-stoichiometry and stability of the materials under reducing conditions are also investigated to ensure that the material would be able to withstand the range of environments encountered during cell construction. Mössbauer spectroscopy has been used to investigate the coordination environment and oxidation state of iron whilst the conduction properties of these materials have been presented elsewhere [14].

2. Experimental

In this work samples ($x = 0.6$–1.0) were synthesized using a citrate gel process as opposed to conventional solid-state synthesis, a method that has not been reported as a synthetic route to these materials. The advantages of this route are well documented and this has frequently been used in the preparation of materials for fuel cell cathodes [14–17]. Stoichiometric quantities of 1 M solutions of the metal nitrates (molarities determined by chemical analysis) were stirred in a beaker. For each mole of transition metal used 3 mol equivalents of citric acid solution were added along with 5 cm^3 of ethylene glycol. The stirred solutions were heated on a hot plate and the liquid was evaporated gradually. A gel was formed and then dehydrated on a hot plate until a black powder residue remained. This residue was ground and calcined in a furnace at 700°C for 12 h to remove any remaining organic components. The resultant powder was subsequently ground and heated in air to 1400°C for 36 h. Reduced samples were prepared by heating as prepared samples in a 10% H_2/N_2 flow at 700°C.

X-ray diffraction, using a Phillips PW1700 series automated powder diffractometer with Cu$K\alpha$ radiation and a graphite secondary crystal monochromator was used to characterize the products at ambient temperature and to check the phase purity of the samples. The oxidation state of the iron and the high-temperature behavior of the materials was investigated using in situ Mössbauer spectroscopy, at the University of Iceland, [18] and iodometric titrations.

High-resolution powder neutron diffraction data were collected using the HRPD beamline at the Rutherford Appleton Laboratories and complemented with high-resolution powder diffraction data recorded in situ at temperature on station 2.3 at the synchrotron radiation source at Daresbury Laboratory.

The reduction of these materials was studied using in situ high-temperature X-ray diffraction at Imperial College, which consisted of a Phillips X'Pert MPD diffractometer with a Bühler HDK 2.4 high-temperature chamber and Cu$K\alpha$ radiation and a graphite secondary crystal monochromator. Also, thermogravimetric analysis using a Stanton Redcroft 780 series simultaneous thermal analyser (TGA/DTA) operating under 10% H_2/N_2 gas flow or in air was used to characterize the reduction process and investigate the oxygen non-stoichiometry of the materials studied.

3. Results and discussion

3.1. Ambient temperatures

X-ray diffraction data were collected using station 2.3 at the synchrotron radiation facility at Daresbury laboratory on powder samples with radiation of wavelength 1.401339 Å and were analyzed by Rietveld refinement using the GSAS suite of programs [18]. The background was fitted with a 6 term shifted Cherbyshev function and the peak shape fitted using a pseudo Voigt function. Data were refined in the space group $I4/mmm$ in common with many La-based K_2NiF_4-type oxides. The K_2NiF_4 structure is illustrated in Fig. 1. La/Sr were randomly distributed over the (00z) site, where $z \approx 0.36$, while Fe occupied (000) and the oxygen atoms were located at $(0\frac{1}{2}0)$ and (00z), where $z \approx 0.16$, positions. The results of this analysis are shown in Table 1 for the $x = 0.8$ composition, where $a = 3.85301(1)$ Å and

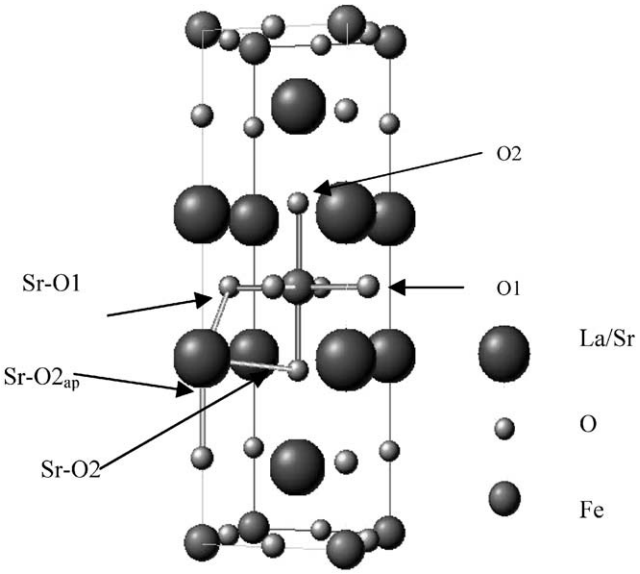

Fig. 1. K_2NiF_4 structure adopted by $La_xSr_{2-x}FeO_{4\pm\delta}$ showing atomic positions and bonds discussed.

Table 1
Structural model of $La_{0.8}Sr_{1.2}FeO_4$

Atom	x	y	z	$U_{iso}\times100$	Occ.
La	0	0	0.35727(8)	0.219(23)	0.38(1)
Sr	0	0	0.35727(8)	0.219(23)	0.62(1)
Fe	0	0	0	0.253(64)	1
O_1	0	0.5	0	0.33(17)	1
O_2	0	0	0.1651(6)	1.52(19)	1

$c = 12.77048(8)$ Å, and Fe–O and (Sr/La)–O bond lengths have been extracted and are given in Figs. 2 and 3.

The results for these citrate gel synthesized samples agree well with the results obtained by Takeda et al. [13] from samples prepared by solid-state routes. Variation in the a cell constant is as expected, Fig. 4, with an increase of the cell constant observed as the La content of the material increases. However, the results for the c cell constant are unusual with an increase as far as the $x = 0.8$ composition and then a marked decrease for $x = 0.9$ and 1.0, Fig. 4. There is also, above the $x = 0.8$ composition, a slight increase in the a constant. The small increase in a as x increases can be understood by assuming a decrease in Fe^{4+} content and an increase in Fe^{3+} in the material as the La^{3+} ions are substituted on the Sr^{2+} site, as Fe^{3+} would form longer Fe–O bonds than Fe^{4+}. The variations in c are determined by a number of competing factors. Substitution of Sr^{2+} by La^{3+} results in shorter La(Sr)–O2 bonds along the c-axis and would be expected to result in a shortening in c. This is consistent for samples with $x>0.8$, however in addition there is the effect of reducing the amount of Fe^{4+} in the structure which should result in an increased Fe–O bond length. If only the change in ionic radii are considered then both Fe–O1 and Fe–O2 bonds should lengthen by similar amounts. However, it is clear from Fig. 2 that this is not the case and that the Fe–O2 bonds are lengthened considerably more than the Fe–O1 bonds, 0.08 and 0.016 Å, respectively.

On reducing the Fe^{4+} ions there are competing factors influencing the bond length changes. The excess electrons generated on the reduction of Fe^{4+} to Fe^{3+} are located in the d_z^2 orbital directed towards the oxygen ions on the (00z) site and extend the Fe–O2 bond length along the c-axis, as discussed by Takeda et al. [13]. Whilst both Fe^{3+} ($d5$) and Fe^{4+} ($d4$) ions could be viewed as having one electron occupying the d_z^2 orbital it is well known that the electron density in the e_g level of the Fe^{4+} containing materials $SrFeO_3$ and $CaFeO_3$ is delocalized [19,20]. Therefore, with the $d4$ ion (Fe^{4+}) it is unlikely that the electron in the e_g level formally occupies either orbital, the d_z^2 or $d_x^2-d_y^2$, but is delocalized as argued by Takeda [13]. Further, previous studies on the Sr_2FeO_4 end member indicated that, although Fe^{4+} would be expected to exhibit Jahn–Teller behavior, the FeO_6 octahedron was only slightly distorted [21,22] indicating that the e_g orbital does not split. This further supports the idea of the Fe^{4+} e_g level being delocalized and *not* subject to Jahn–Teller distortion. Therefore, it may be assumed that on reduction of Fe^{4+} to Fe^{3+} both the d_z^2 and $d_x^2-d_y^2$ orbitals will be formally occupied as the e_g orbital losses its degeneracy and hence the lengthening of the Fe–O2 bonds along which the d_z^2 orbitals are located can be attributed to the excess electrons being localized in the d_z^2 orbital. Further discussion of the electronic structure of Fe^{4+} containing materials is provided in Refs. [19,20].

The oxygen atom on (00z) is thus displaced along c away from the iron atom and towards the (La, Sr) site and therefore the FeO_6 octahedron increases in size as Fe^{4+} is reduced. Fig. 2 clearly shows an increase in the Fe–O2 bond length from $x = 0.7$ onwards consistent with this while Fig. 3 shows the Sr–$O2_{ap}$ (where ap = apical) bond length decreasing after the $x = 0.7$ composition. However, on closer examination it is evident that both bond lengths change by approximately the same value, 0.08 Å, and so should not affect the c-axis as the bond lengthening and shortening effects cancel one another out. However, the (La, Sr)–O1 bonds also decrease in length as shown in Fig. 3 and it is this which is of greater significance. Effectively the distance between the rocksalt and perovskite layers is decreasing and this is the important factor leading to the abrupt change observed in the length of the c-axis after the composition $x = 0.8$.

Looking at the intimate structure there are three distinct (La, Sr)–O bonds. One is in the perovskite layer, one is in the rocksalt layer in the ab plane and the third

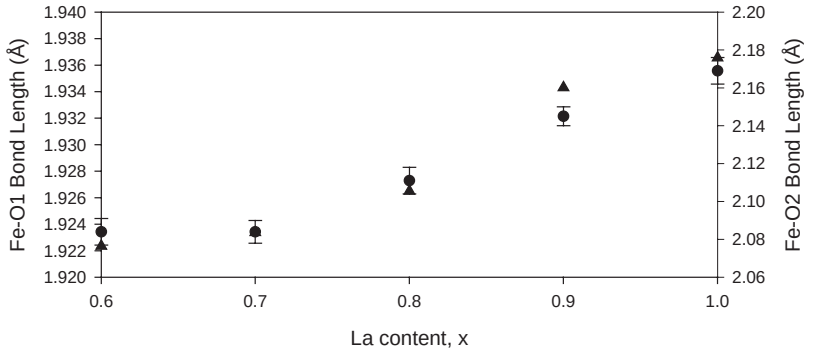

Fig. 2. Fe–O1 and Fe–O2 bond lengths as a function of composition.

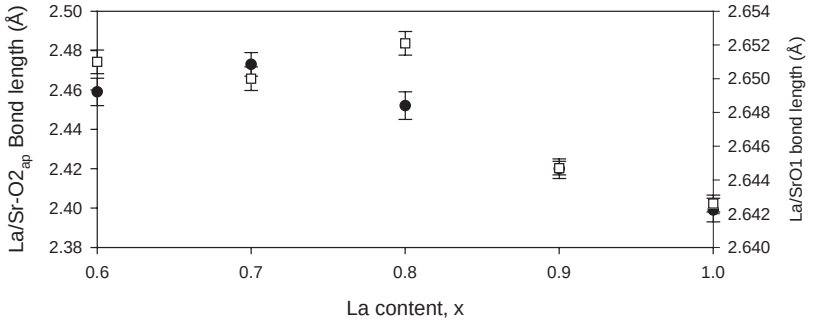

Fig. 3. La/Sr–$O2_{ap}$ and La/Sr–O1 bond length variation with La composition calculated from synchrotron XRD data.

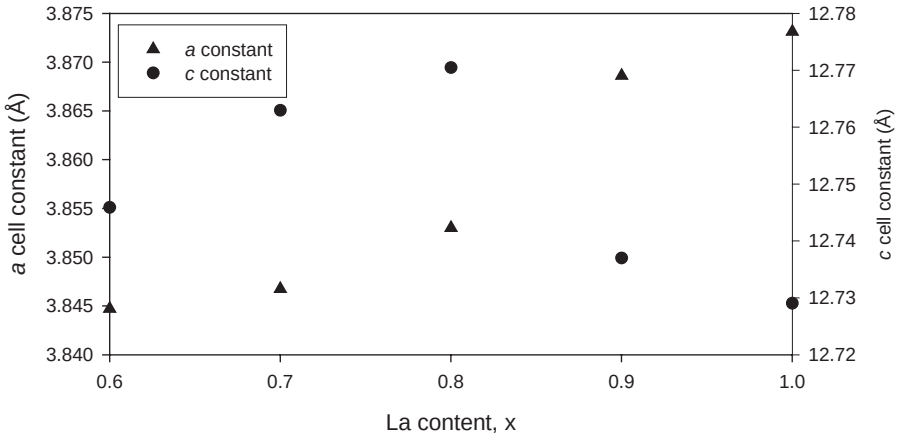

Fig. 4. Variation with composition of cell constants refined from data collected using synchrotron XRD. Triangles indicate *a* cell constant and circles indicate *c* cell constant (errors are within data markers).

is the bond in the rocksalt layer along the *c*-axis as depicted in Fig. 1. These bonds are affected differently by changes in the composition. As the amount of Fe^{3+} in the sample increases (*x* increases) more electrons are introduced into the d_z^2 orbitals on the iron atoms. The d_z^2 orbitals are directed along the *c*-axis, as previously discussed, and the repulsion between these electrons and the oxygen atom in the apical plane results in a lengthening in the Fe–O2 bond length and hence a decrease in the (La, Sr)–$O2_{ap}$ bond length in this direction. Hence, this bond is significantly affected by changes in the composition of the sample in terms of the La/Sr ratio. The corresponding Fe–O2 bond lengths can also be seen to vary significantly. These effects balance out with the increase in the Fe–O2 bond length and decrease in the (La, Sr)–$O2_{ap}$ bond length being of similar magnitude. The (La, Sr)–O1 bond length also decreases as La content increases and these changes are of similar magnitude to the changes in the other bond lengths.

TGA data recorded from these materials showed that when heated in dry air samples gained some mass which could be attributed to oxygen uptake and then on cooling the mass gained was subsequently lost. This indicated that the samples adopted variable oxygen stoichiometry, which was temperature dependent. A large mass gain was observed starting at 600°C and peaking at 800°C followed by a sharp decrease. This behavior was observed, in particular, for samples with $x = 0.6$, 0.7 and 0.8 and to a smaller extent for $x = 0.9$. This suggested that as the Fe^{4+} content was reduced, so the flexibility in oxygen stoichiometry was lost. It is also significant that this behavior was observed at the composition at which the *c*-parameter decreased indicating, perhaps, that those samples with higher Fe^{3+} contents could not be easily oxidized.

3.2. In situ high-temperature diffraction data

Variable temperature neutron diffraction data were collected for the $x = 0.9$ sample with the aim of confirming that there were no subtle structural transitions occurring on heating the sample and also of examining in detail variations in the structure, and in particular bond lengths, on heating and cooling. Full Rietveld refinements were performed on the data collected and these indicated that the K_2NiF_4-type structure was maintained on heating but that some unusual changes occurred in the bonding within the structure. Each data set was refined in the $I4/mmm$ space group as previously described and typical data are presented in Table 2 and Fig. 5. The *a* and *c* cell constants increased linearly with temperature as shown in Fig. 6. However, these apparently simple results mask unusual changes in the bond lengths within the sample with temperature. Figs. 7 and 8 show the variation in the Fe–O and (La, Sr)–O bond lengths respectively with temperature. While the Fe and La/Sr bonds to O1 varied linearly, the bonds to O2, and in particular the bonds in the *c*-axis direction showed no such linear variation. This indicates that the optimum location of the oxygen with respect to the La/Sr and Fe atoms changed with temperature.

There are four temperature regimes in which bond length variations can be allocated. Between 0°C and 200°C, the Fe–O2 bond lengthens linearly with temperature while the (La, Sr)–$O2_{ap}$ bond length decreases. Between 200°C and 500°C there was no change in the Fe–O2 bond length but the (La, Sr)–$O2_{ap}$ bond length increased. From 500°C to 600°C the Fe–O2 bond length now increased while the (La, Sr)–$O2_{ap}$ bond length is unchanged. Finally, after 600°C,

Table 2
Refined data for $La_{0.9}Sr_{1.1}FeO_4$ at 25°C from HRPD data

	x	*y*	*z*	$U_{iso} \times 100$	Occ.
La	0	0	0.35785(8)	0.91(4)	0.442(8)
Sr	0	0	0.35785(8)	0.91(4)	0.547(8)
Fe	0	0	0	1.305	1
O_1	0	0.5	0	1.182	0.980(8)
O_2	0	0	0.16861(12)	2.121	0.978(8)

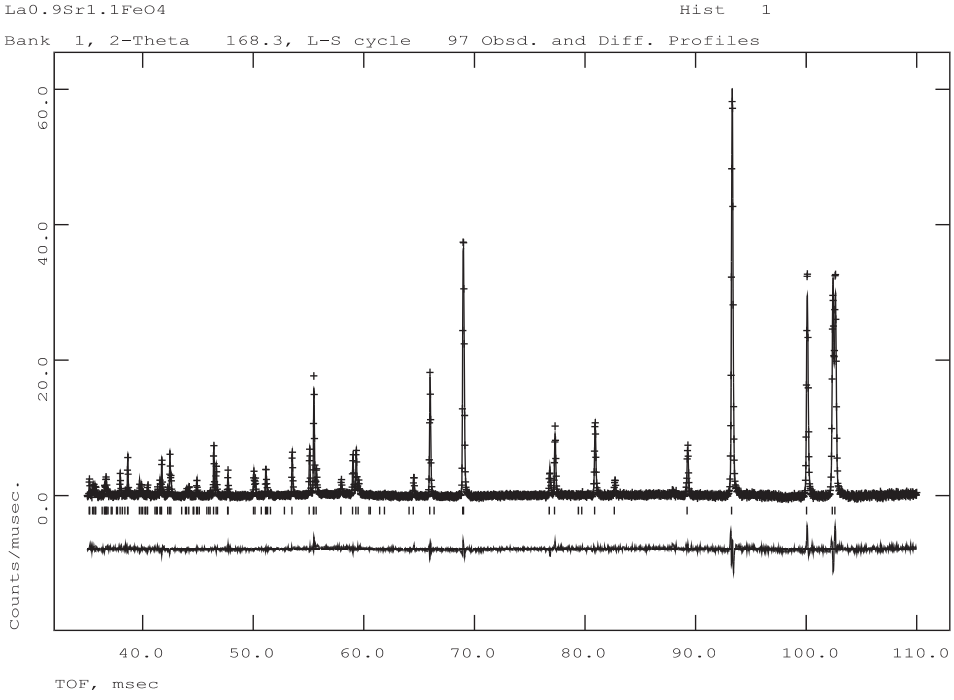

Fig. 5. Rietveld refinement of $La_{0.9}Sr_{1.1}FeO_{4\pm\delta}$ from HRPD data. $R_{wp} = 6.25$, $R_p = 5.17$ and $\chi^2 = 2.00$.

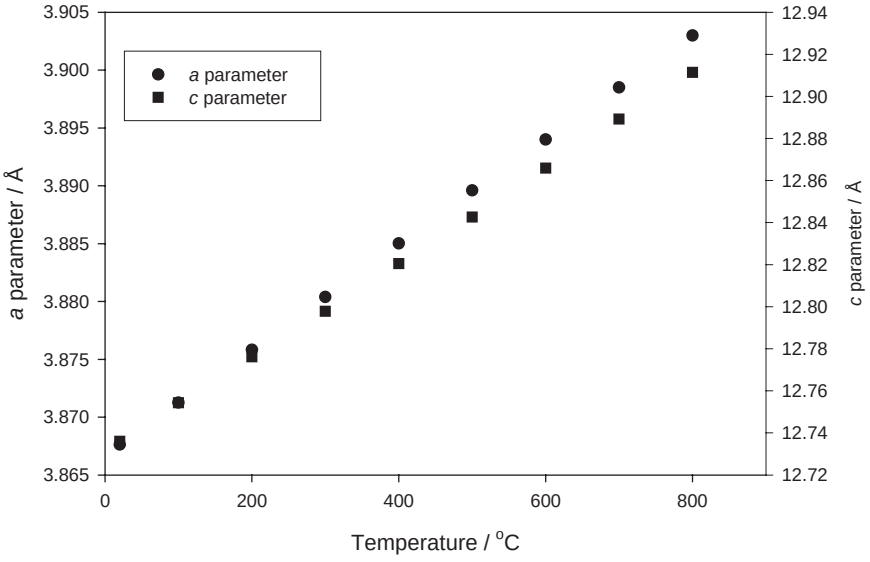

Fig. 6. Variation of *a* and *c* cell parameters as a function of temperature determined from powder neutron diffraction data for the $La_{0.9}Sr_{1.1}FeO_{4\pm\delta}$ composition.

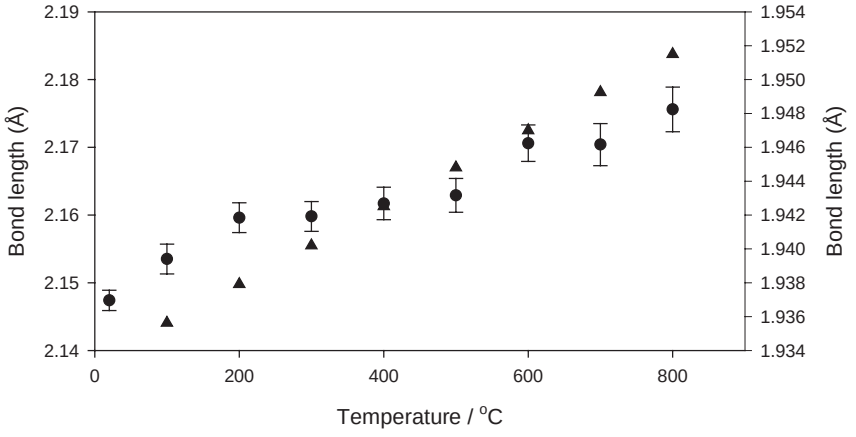

Fig. 7. Fe–O1 and Fe–O2 bond lengths as a function of temperature refined from powder neutron diffraction data for $La_{0.9}Sr_{1.1}FeO_{4\pm\delta}$. (Where no error bars are shown the errors are within the data markers.)

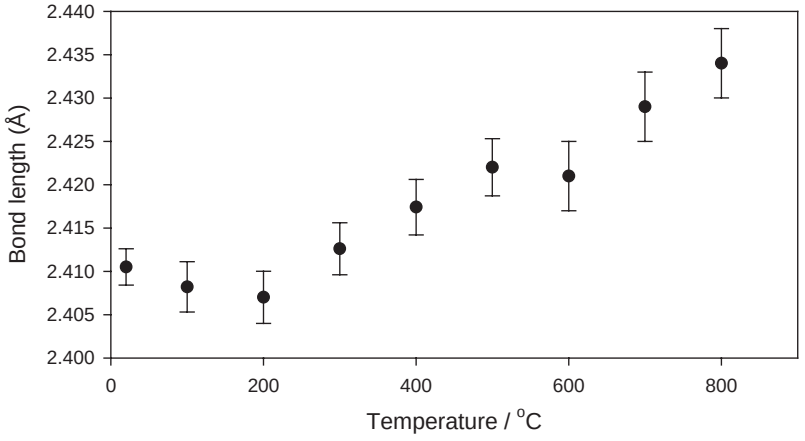

Fig. 8. (La, Sr)–O bond lengths as a function of temperature refined from powder neutron diffraction data for the $La_{0.9}Sr_{1.1}FeO_{4\pm\delta}$ composition.

both bond lengths increased. These results indicate that anisotropic thermal expansion occurred in these materials up to 600°C.

It should also be noted that the temperature factor on the oxygen atom O2 refined to a relatively high value in all of the refinements. This appears to be a feature of this system as analysis of synchrotron and other X-ray data for this and other compositions shows the same behavior. If the temperature factor is refined anisotropically an ellipsoid results that is elongated in the *ab* plane. This suggests that the oxygen atoms could be mobile in the *ab* plane at the temperatures under which the material was studied although further measurements would be required to verify this. However, this has been observed in similar K_2NiF_4 structured materials [23–25] in which oxide ion mobility was subsequently reported.

3.3. Reduced samples

The reduction of the $La_xSr_{2-x}FeO_{4\pm\delta}$ samples was investigated using in situ high-temperature X-ray diffraction and the results indicated that on heating in 10% H_2/N_2 gas flow significant oxygen loss occurred that resulted in an increase in both the *a* and *c* unit-cell parameters when compared to the same sample heated in air as shown in Fig. 9 for the $La_{0.7}Sr_{1.3}FeO_{4\pm\delta}$ composition. On reheating the reduced sample in air full re-oxidation was observed as evidenced by the change of the lattice parameters and similar results were observed for all of the materials examined in this work, $La_xSr_{2-x}FeO_{4\pm\delta}$, $x = 0.6-1.0$. The reduction step can be attributed to the reduction of Fe^{4+} to Fe^{3+} and corresponding loss of oxygen from the structure.

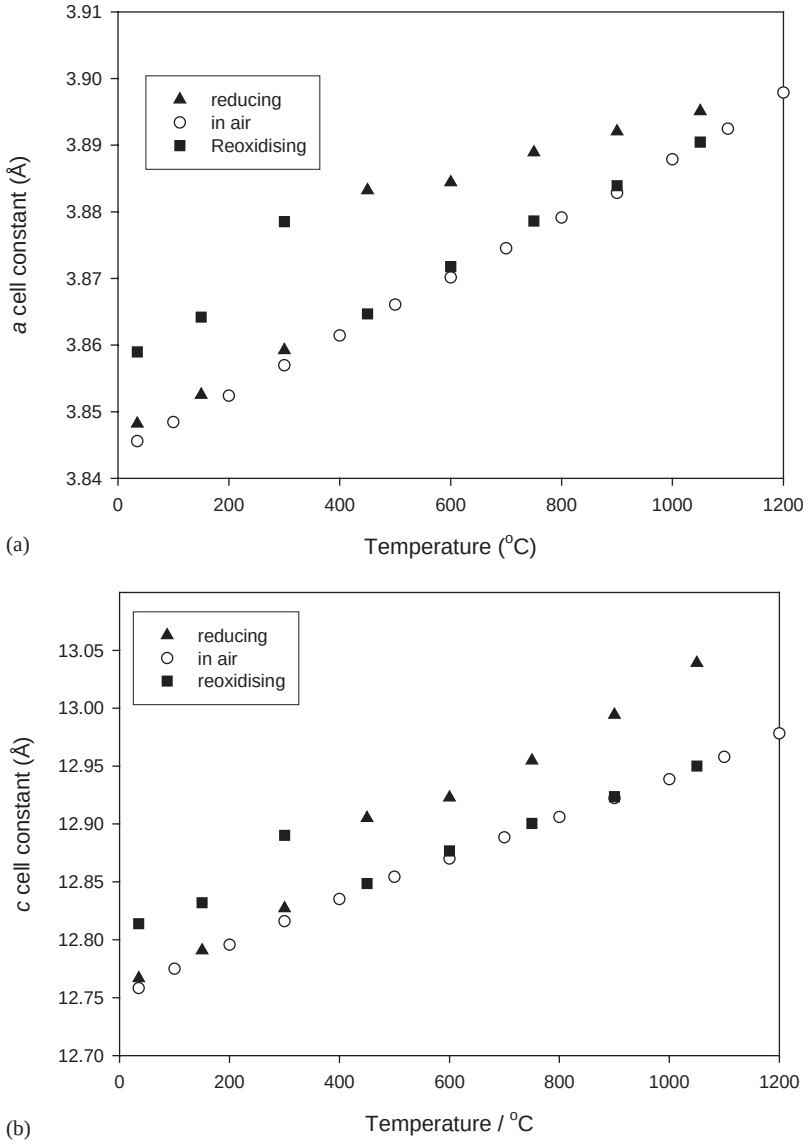

Fig. 9. Cell constants (a) *a* and (b) *c* determined for $La_{0.7}Sr_{1.3}FeO_{4\pm\delta}$ from X-ray data as a function of temperature and atmosphere. Triangles indicate data collected in air, squares in H_2/N_2 gas flow and circles in air reoxidizing the sample.

The in situ diffraction data collected during the reduction process showed that the reduction step occurred at around 450°C and this was in agreement with TGA results. From the calculated unit-cell constants it was apparent that at 450°C a large increase in the *a* cell constant occurred, Fig. 9a. After further heating the unit-cell data indicated that further increases in the *a* parameter were due to linear thermal expansion of the sample. By contrast the *c* cell constant varied linearly with temperature across the entire temperature range, 25–1000°C. On close examination of the diffraction data, both before and after reduction, at ambient temperature, it is clear that both *a* and *c* parameters are 0.5% larger after reduction.

To investigate variations of the structure of the reduced samples with composition in detail, data were collected using synchrotron X-ray diffraction at station 2.3 at Daresbury laboratory. Rietveld refinements of the data using the K_2NiF_4 type structure, as previously, resulted in good fits and gave the data shown in Table 3 and Fig. 10 for $x = 0.8$ composition. For the compositional range $0.9 \leqslant x \leqslant 0.6$ the cell constants were found to vary linearly with composition in contrast to the non-linear variations observed for the unreduced materials, Fig. 4. The *a* and *c* unit-cell parameters were found to be generally larger for the reduced samples when compared to the data obtained from the oxidized materials, Table 4. Similar but more exaggerated behavior was observed by Li and Greaves for the manganite $La_{1.2}Sr_{0.8}MnO_{4\pm\delta}$ [23]. The results of the refinements also indicated that there was a small loss of oxygen from both sites, O1 and O2 corresponding to an overall oxygen deficiency of $\delta = 0.29$ for the $x = 0.8$ composition.

Table 3
Refined data for $La_{0.8}Sr_{1.2}FeO_{4-\delta}$ reduced sample

	x	*y*	*z*	$U_{iso}\times100$	Occ.
La	0	0	0.35778(8)	0.378(29)	0.4
Sr	0	0	0.35778(8)	0.378(29)	0.6
Fe	0	0	0	0.13(6)	1
O_1	0	0.5	0	0.3(3)	0.931(18)
O_2	0	0	0.1653(7)	2.6(4)	0.926(19)

The variation in the unit-cell constants can be considered to be due to the reduction process. After reduction all of the iron is in the +3 oxidation state and therefore the (La, Sr)–O bond lengths have a dominating effect on the *c* cell constant. Samples with higher La contents exhibit shorter (La, Sr)–O bond lengths and this is in direct proportion to *x*. The *a* cell constants are dominated by the Fe–O bond lengths. All are higher in the case of the reduced samples when compared to oxidized samples due to the longer bond lengths formed by Fe^{3+} to oxygen compared to Fe^{4+}. Therefore, an increase in the unit-cell parameters on reduction is unsurprising.

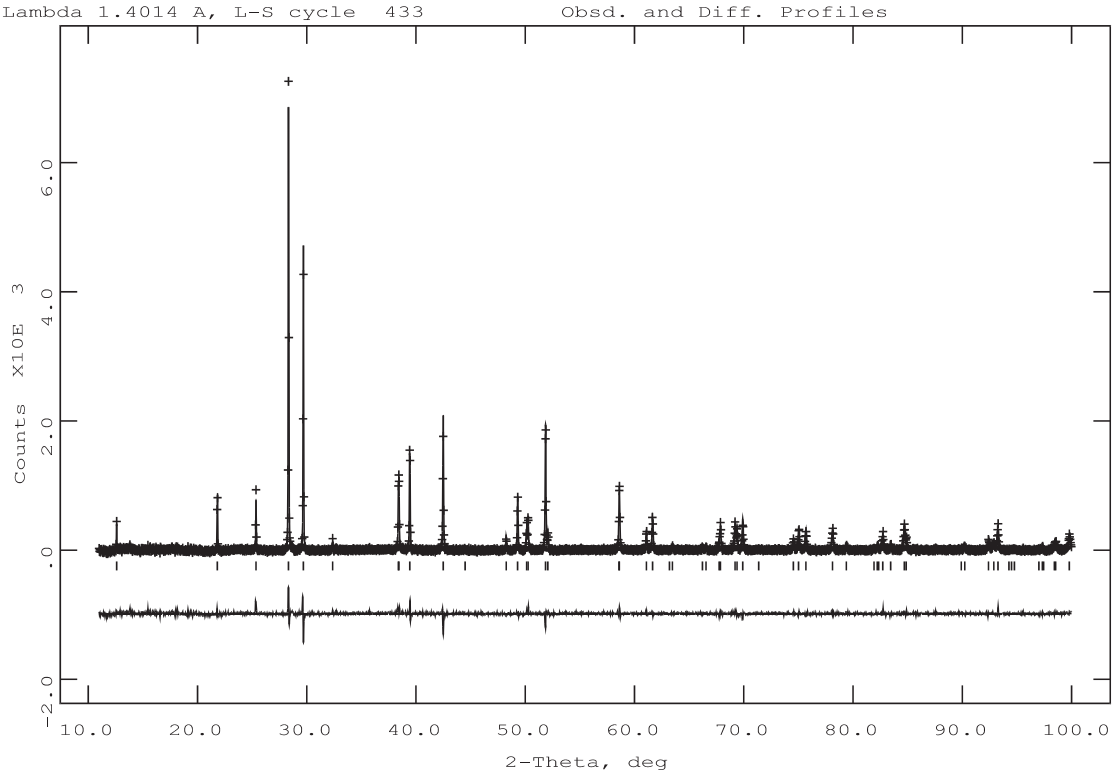

Fig. 10. Rietveld refinement of $La_{0.8}Sr_{1.2}FeO_{4\pm\delta}$ reduced phase. $R_{wp} = 9.99$, $R_p = 7.75$ and $\chi^2 = 1.682$.

Table 4
Comparison of reduced and oxidised lattice parameters for $La_xSr_{2-x}FeO_{4\pm\delta}$

x	a_{red} (Å)	a_{oxid} (Å)	Diff. (Å)	c_{red} (Å)	c_{oxid} (Å)	Diff. (Å)
0.6	3.85556	3.84470	0.01086	12.8138	12.7459	0.0679
0.7	3.86108	3.84675	0.01433	12.8048	12.7629	0.0419
0.8	3.86729	3.85301	0.01428	12.7693	12.7705	−0.0012
0.9	3.87347	3.86861	0.00486	12.7384	12.7370	0.0014

Table 5
Results of iodometric titrations and TGA

Nominal comp.	Titrations	TGA
$LaSrFeO_4$	$LaSrFe^{III}_{0.89}Fe^{IV}_{0.11}O_{4.05}$	$LaSrFe^{III}_{0.92}Fe^{IV}_{0.08}O_{4.04}$
$La_{0.9}Sr_{1.1}FeO_4$	$La_{0.85}Sr_{1.12}Fe^{III}_{0.86}Fe^{IV}_{0.14}O_{3.97}$	$La_{0.85}Sr_{1.12}Fe^{III}_{0.86}Fe^{IV}_{0.14}O_{3.96}$
$La_{0.8}Sr_{1.2}FeO_4$	$La_{0.8}Sr_{1.2}Fe^{III}_{0.78}Fe^{IV}_{0.22}O_{4.01}$	$La_{0.8}Sr_{1.2}Fe^{III}_{0.80}Fe^{IV}_{0.20}O_{3.99}$
$La_{0.7}Sr_{1.3}FeO_4$	$La_{0.7}Sr_{1.3}Fe^{III}_{0.71}Fe^{IV}_{0.29}O_{3.99}$	$La_{0.7}Sr_{1.3}Fe^{III}_{0.69}Fe^{IV}_{0.31}O_{4.01}$
$La_{0.6}Sr_{1.4}FeO_4$	$La_{0.6}Sr_{1.4}Fe^{III}_{0.56}Fe^{IV}_{0.44}O_{4.02}$	$La_{0.6}Sr_{1.4}Fe^{III}_{0.54}Fe^{IV}_{0.46}O_{4.03}$

3.4. Oxygen stoichiometry and Mössbauer spectroscopy

The results of iodometric titrations are presented in Table 5. All samples were found to contain Fe^{4+} in varying proportions and to be fully oxygen stoichiometric except for those that had been subjected to the reducing heat treatments. The amount of Fe^{4+} present in the samples increased as x decreased, as expected, and in accordance with previous work by Takeda et al. [13]. There is no evidence in these samples for the presence of interstitial oxide ions, which would result in a larger proportion of Fe^{4+} being present. This is also in agreement with the results of the earlier Rietveld refinement process in which no interstitial position could be fitted to the neutron diffraction data recorded from the oxidized material.

^{57}Fe Mössbauer spectroscopy confirmed the presence of Fe^{4+} in these materials. Mössbauer spectra recorded from samples of various compositions, at ambient temperature and also at elevated temperatures were characterized by a quadrupolar doublet. A best fit to the data was obtained with a two component model as shown for one sample, $La_{0.8}Sr_{1.2}FeO_{4\pm\delta}$, in Fig. 11. Several models were used in an attempt to fit the doublet. Initially a single doublet was used but the fit was poor and the peak width much larger than that expected of between 0.3 and 0.4 mm s^{-1}. Hence, a two doublet fit was used to fit the spectra. There are two possible fits to the data. In the first model the quadrupole splittings (QS) of the doublets were similar and the isomer shifts (IS) very different and in the second model the IS were of similar value while the QS were now very different. Both models showed doublets with sensible peak widths ($\sim$0.3–0.4 mm s^{-1}). The first model most appropriately fits the data and gives the most physically sensible model. This model implies two different formal Fe oxidation states. The IS values obtained for $LaSrFeO_{4\pm\delta}$ at 12°C of 0.17 and 0.38 mm s^{-1} would correspond to a formally mixed Fe^{3+}/Fe^{4+} component and an Fe^{3+} component, respectively. There are a number of examples in the literature of similar materials displaying these IS. Model 2 is unlikely as the two values for the IS are 0.30 and 0.29 mm s^{-1}. In this case the different QS values would suggest that the Fe would occupy more than one chemical environment and the detailed structural work we have performed using synchrotron X-ray and neutron diffraction suggests that there is only one iron environment in these materials. Hence, model 1 has been adopted to analyze the data on all the samples.

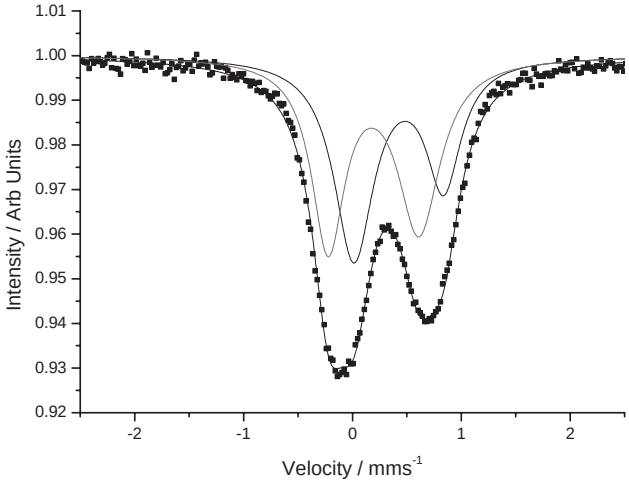

Fig. 11. ^{57}Fe Mössbauer spectroscopy data recorded from $La_{0.8}Sr_{1.2}FeO_{4\pm\delta}$ illustrating the two quadrupolar doublet model used.

Table 6
^{57}Fe Mössbauer results at 12°C

La content, x	Component 1				Component 2			
	IS (mm s^{-1})	QS (mm s^{-1})	W	%	IS (mm s^{-1})	QS (mm s^{-1})	W	%
0.7	0.17(1)	0.68(1)	0.40(1)	50(2)	0.41(1)	0.72(1)	0.39(1)	49(2)
0.8	0.19(1)	0.83(1)	0.42(1)	52(2)	0.42(1)	0.82(1)	0.42(1)	47(2)
1.0	0.17(1)	0.92(1)	0.32(1)	39(2)	0.38(1)	0.94(1)	0.40(1)	60(2)

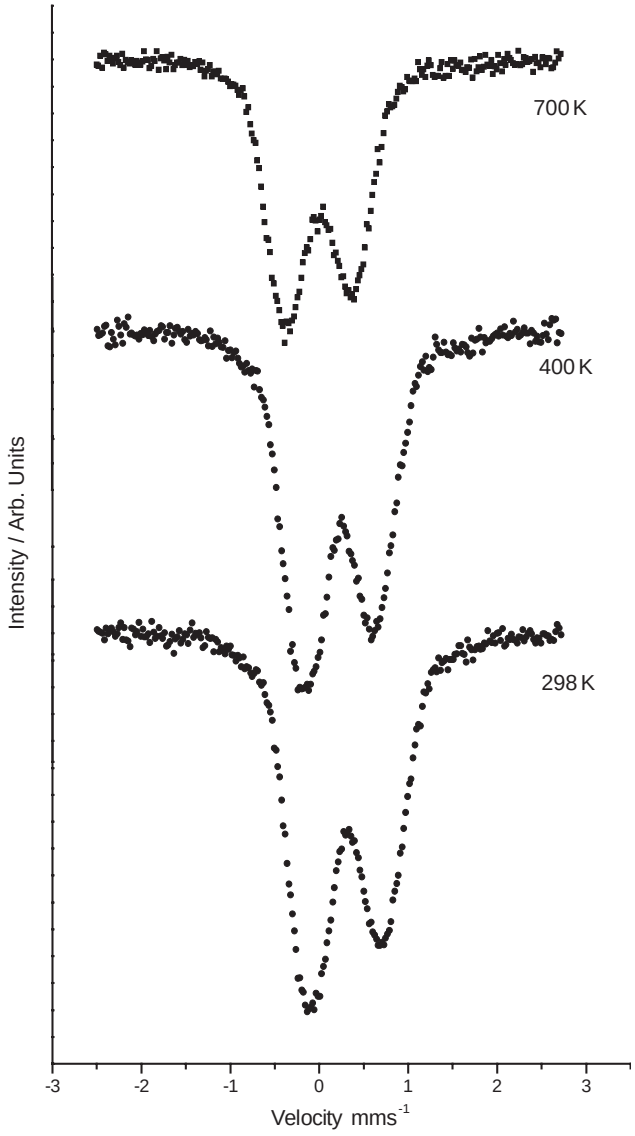

Fig. 12. ^{57}Fe Mössbauer spectra for $La_{0.8}Sr_{1.2}FeO_{4\pm\delta}$ recorded at 298, 400 and 700 K illustrating the offset in isomer shift observed on heating.

All of the samples measured showed similar results. The fitted parameters are presented in Table 6. From these data it can be seen that the proportion of Fe^{4+} in the samples varies slightly with composition as expected and as also observed in the chemical analysis. The values of the quadrupolar shift vary markedly with composition. For example at 12°C the Fe^{3+} component has QS values of 0.72, 0.82 and 0.94 mm s^{-1} for the $x = 0.7$, 0.8 and 1.0 samples, respectively. The QS value is related to the bonding environment around the Fe atom. In the K_2NiF_4 structure the Fe is bound to six oxygen atoms. As discussed in the structural analysis the geometry of the octahedron formed is distorted such that the apical Fe–O bonds are elongated with respect to the equatorial Fe–O bonds as the Fe^{3+} content of the material increases. Elongation of the bonds results in the higher QS values reported.

Variable temperature Mössbauer spectroscopy was performed in air at a pressure of 1 atm. These data showed a movement in the isomer shift value with temperature, Fig. 12. For both the Fe^{3+} and Fe^{3+}/Fe^{4+} components the isomer shift decreases with temperature linearly according to 0.0007 mm s^{-1} K^{-1}. For a given temperature the isomer shift value is unchanged for the two individual components with composition. Hence, we can be confident that there is in fact only one iron site in these structures. There is no evidence for a change in the coordination sphere of the iron which would be expected with the incorporation of excess oxygen in these samples.

These results are in agreement with Omata et al. [9,10], who find that for $x = 0.9$ there is a doublet in the room temperature spectrum which is best fitted by two superimposed doublets. They assigned one doublet with IS = 0.38 mm s^{-1} and QS = 0.93 mm s^{-1} as Fe^{3+} and a second component with IS = 0.16 mm s^{-1}, QS = 0.87 mm s^{-1} and as a mixture of Fe^{3+} and Fe^{4+} oxidation states.

4. Conclusions

These materials exhibit variable oxygen stoichiometry. Under certain conditions, for example, at elevated temperature and under oxidizing conditions, it appears that excess oxygen may be present in these materials in the form of interstitials. Also it was found that under reducing conditions, 10%H_2/N_2, these samples were relatively stable. Furthermore, a large amount of lattice oxygen can be removed from the structure leading to vacancy formation and a reduction of the iron from +4

to +3 oxidation state. This then leads to a wide range of possible oxygen stoichiometries although the evidence from Mössbauer spectroscopy, iodometric titrations and structural refinements suggests that samples made in air are stoichiometric $La_xSr_{2-x}FeO_4$, at ambient temperature.

The tetragonal K_2NiF_4 structure was maintained at high temperatures as evidenced by in situ high-temperature X-ray diffraction, neutron diffraction and Mössbauer spectroscopy studies. Only one unique iron site and no evidence to support the presence of an interstitial oxide ion site was found from the detailed structural investigations.

Acknowledgments

We thank EPSRC for the funding of this project through grant number GR/N23233 and also for the award of beam-time at Daresbury laboratory, reference number 37101, and Rutherford Appleton laboratory, reference RB12502. Thanks are also due to Dr. C. Tang, Daresbury, and Dr. K. Knight, Rutherford, for their valuable assistance with the data collection. Thanks are also due to Mr. Richard Sweeney, Imperial College, for assistance with the high-temperature X-ray diffraction facility.

References

[1] V.V. Kharton, A.P. Viskup, A.V. Kovalevsky, E.N. Naumovich, F.M.B. Marques, Solid State Ionics 143 (2001) 337.
[2] V.V. Kharton, A.P. Viskup, E.N. Naumovich, F.M.B. Marques, J. Mater. Chem. 9 (1999) 2623.
[3] S.J. Skinner, J.A. Kilner, Solid State Ionics 135 (2000) 709.
[4] H. Zhang, J. Jin, G.Y. Yu, N.R. Yang, J.L. Shi, J.W. Feng, J. Inorg. Mater. 16 (2001) 440.
[5] H. Zhang, J. Jin, G.Y. Yu, N.R. Yang, X.Y. Zhou, Chin. J. Inorg. Chem. 16 (2000) 911.
[6] L. Minervini, R.W. Grimes, J.A. Kilner, K.E. Sickafus, J. Mater. Chem. 10 (2000) 2349.
[7] V.V. Vashook, N.E. Trofimenko, H. Ullmann, L.V. Makhnach, Solid State Ionics 131 (2000) 329.
[8] J.A. Kilner, C.K.M. Shaw, Solid State Ionics 154–155 (2002) 523–527.
[9] T. Omata, K. Ueda, N. Ueda, M. Katada, S. Fujitsu, T. Hashimoto, H. Kawazoe, Solid State Commun. 88 (1993) 807.
[10] T. Omata, K. Ueda, H. Honso, M. Katada, N. Ueda, H. Kawazoe, Phys. Rev. B 49 (1994) 10194.
[11] M. Shimada, M. Koizumi, Mater. Res. Bull. 11 (1976) 1237.
[12] J.L. Soubeyroux, P. Courbin, L. Fournes, D. Fruchart, G. Le Flem, J. Solid State Chem. 31 (1980) 313.
[13] Y. Takeda, K. Imayoshi, N. Imanishi, O. Yamamoto, M. Takano, J. Mater. Chem. 4 (1994) 19.
[14] A.J. Jennings, S.J. Skinner, Solid State Ionics 152–153 (2002) 663.
[15] D. Waller, J.A. Lane, J.A. Kilner, B.C.H. Steele, Mater. Lett. 27 (1996) 225.
[16] G.C. Kostogloudis, C. Ftikos, Solid State Ionics 126 (1999) 143.
[17] A.V. Berenov, J.L. MacManus-Driscoll, J.A. Kilner, Solid State Ionics 122 (1999) 41.
[18] A.C. Larson, R.B. Von Dreele, General Structure Analysis System, Los Alamos National Laboratory, 1995.
[19] A.E. Bocquet, A. Fujimori, T. Mizokawa, T. Saitoh, H. Namatame, S. Suga, N. Kimizuka, Y. Takeda, M. Takano, Phys. Rev. B 45 (1992) 1561.
[20] M. Takano, S. Nasu, T. Abe, K. Yamamoto, S. Endo, Y. Takeda, J.B. Goodenough, Phys. Rev. Lett. 67 (1991) 3267.
[21] S.E. Dann, M.T. Weller, D.B. Currie, J. Solid State Chem. 96 (1991) 237.
[22] S.E. Dann, M.T. Weller, D.B. Currie, J. Solid State Chem. 97 (1992) 179.
[23] R.K. Li, C. Greaves, J. Solid State Chem. 153 (2000) 34.
[24] H. Lui, Y. Ge, P. Chen, M. Mei, F. Ma, G. Lu, J. Mater. Chem. 7 (1997) 2097.
[25] J.E. Millburn, M.J. Rossiensky, Chem. Mater. 9 (1997) 511.